Report no. 08/16

Conformal Maps to Multiply-Slit Domains and Applications

Nicholas Hale T. Wynn Tee

By exploiting conformal maps to vertically slit regions in the complex plane, a recently developed rational spectral method [27] is able to solve PDEs with interior layer-like behaviour using significantly fewer collocation points than traditional spectral methods. The conformal maps are chosen to 'enlarge the region of analyticity' in the solution: an idea which can be extended to other numerical methods based upon global polynomial interpolation. Here we show how such maps can be rapidly computed in both periodic and nonperiodic geometries, and apply them to some challenging differential equations.

Oxford University Computing Laboratory
Numerical Analysis Group
Wolfson Building
Parks Road
Oxford, England OX1 3QD

October, 2008

1 Introduction

Numerical methods based upon global interpolation perform well when the underlying solution is sufficiently smooth. For example, when a real function f can be continued analytically to the closed ellipse E_ρ with foci ± 1 and semiaxis lengths that sum to ρ, the Chebyshev spectral method using $N+1$ collocation points approximates the derivative of f on $[-1,1]$ with an error that decays at a rate $O(\rho^{-N})$ as $N \to \infty$ [25]. Often, such rapid convergence means only a few degrees of freedom are necessary to achieve a high degree of accuracy, but if f has singularities in the complex plane close to $[-1,1]$ so that $\rho \approx 1$, convergence can be too slow for the method to be effective.

However, in these situations it is often the case that f may be continued analytically into a larger, non-elliptical region. By constructing a suitable conformal map g to such a region, the largest ellipse with foci ± 1 in which $f \circ g$ is analytic can be made larger than that of f alone, and applying the numerical method to $f \circ g$ will result in an improved convergence rate. This idea of 'enlarging the ellipse of analyticity' was exploited with convincing results in the adaptive rational spectral method of Tee and Trefethen [27], and the transplanted quadrature methods of Hale and Trefethen [18]. Figure 1 shows the result of applying one such map g in the linear rational spectral method of Berrut et al. [3] when approximating the first derivative of the Runge-type function $f(x) = 1/(1+400x^2)$ on $[-1,1]$.

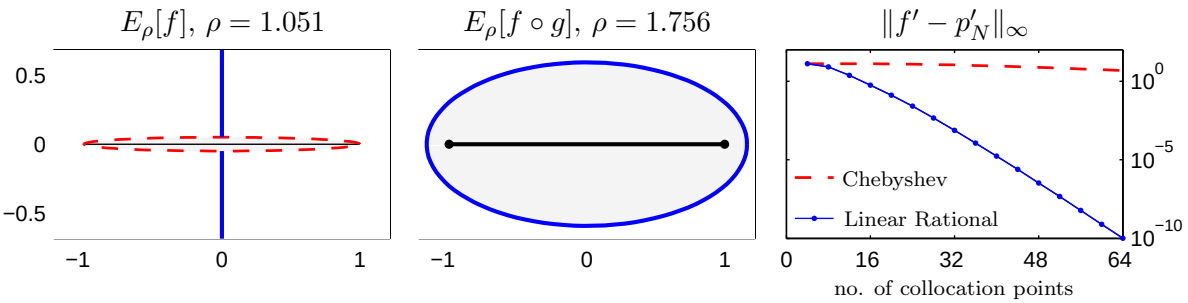

Figure 1: The function $f(x) = 1/(1+400x^2)$ has singularities at $\pm 0.05i$, making the largest ellipse in which it is analytic very narrow (left, dashed). By finding a conformal map from an ellipse to the slit plane (left, solid), the composition $f \circ g$ is analytic in a much larger ellipse (centre). The improvement over the standard Chebyshev spectral method in approximating the derivative by using the linear rational collocation method [3] with this map g is dramatic (right).

The question remains as to how such a map g should be constructed, and to narrow the countless number of possibilities it is necessary to make further assumptions about the properties of f. In [27] it is assumed that f is analytic in the entire complex plane except along a pair of vertical slits extending from complex conjugate points to infinity, an assumption which accounts for a number of scenarios such as when f has poles or branch points with a common real part. The purpose of this paper is to present maps allowing the more general situation, where not just one but multiple pairs of vertical

slits are removed from the complex plane.

In §2 we present such maps suitable for methods based upon algebraic polynomial interpolation, which were originally considered in the second author's doctoral thesis [26]. We show that due to the special geometry of these slit regions, the integrals in the Schwarz–Christoffel formulation of the maps can be computed analytically. Further we describe how the maps may be expressed in such a way that half of the unknowns in the parameter problem enter only linearly, allowing both a fast and accurate computation.

In §3 we turn our attention to periodic analogues of these multiple-slit maps, which can be applied to numerical methods based upon trigonometric polynomial interpolation. Using what we believe to be a new technique loosely based on Schwarz–Christoffel ideas, the map to a periodically repeating sets of conjugate slits is again expressed in an explicit form with a reduced parameter problem.

Finally, as the example and discussion above suggests, we are motivated in this work by practical applications involving the solution of differential equations. In §4 we apply the multiple-slit maps within the linear and adaptive rational spectral methods [3, 27] to solve some challenging near-singular ordinary and partial differential equations.

2 Ellipse to Infinite Slits

We have mentioned already the importance of the ellipse with foci ± 1 in determining the geometric convergence of the Chebyshev spectral method for analytic functions, but this ellipse E_ρ appears also within convergence results of other polynomial based methods. Gauss and Clenshaw–Curtis quadrature [5, 23] and Legendre spectral methods [9] for example each converge geometrically at a rate determined by ρ, which can be seen as a consequence of rapidly decreasing Chebyshev coefficients and rapidly converging best polynomial approximations for functions analytic in this region [29, §4]. In order to improve convergence rates of such numerical methods as those above by enlarging the region of analyticity in the manner suggested in the introduction, we seek conformal maps from the ellipse to slit regions in the complex plane. We consider first mapping to only a single pair of conjugate slits

$$S_{\delta+i\varepsilon} = \mathbb{C} \setminus \{[\delta - i\varepsilon, \delta - i\infty] \cup [\delta + i\varepsilon, \delta + i\infty]\}, \quad \varepsilon > 0, \tag{2.1}$$

but then allow more generality with multiple slits $S_{\{\underline{\delta}+i\underline{\varepsilon}\}}$ with tips at $\{\delta_k \pm i\varepsilon_k\}_{k=1}^n$.

To achieve this, we make use of two important conformal mapping tools; the Schwarz–Christoffel formulae and the Schwarz reflection principle. If $\mathcal{P}$ is a polygon with vertices $w_1, w_2, \ldots, w_n$ and interior angles $\alpha_1\pi, \alpha_2\pi, \ldots, \alpha_n\pi$, the Schwarz–Christoffel formula for the disk [11, (2.4)]

$$h(z) = A + C \int^z \prod_{k=1}^{n} \left(1 - \frac{\xi}{z_k}\right)^{a_k - 1} d\xi, \tag{2.2}$$

defines a conformal map h from the unit disk to the interior of $\mathcal{P}$, where A and C are complex constants and $z_1, z_2, \ldots, z_n$ are prevertices such that $h(z_k) = w_k$ for $k = 1, 2, \ldots, n$. There are two main difficulties associated with computing conformal maps

from Schwarz–Christoffel formulae; integrating the right-hand side of (2.2), and the so-called *parameter problem* of determining prevertices so that $h(z_k) = w_k$ is satisfied. Numerical quadrature is usually required to evaluate the integral and in general the parameter problem is nonlinear with no analytic solution; thus solving the system of equations for the prevertices can be a computationally expensive process. Finding an explicit expression by evaluating the integral analytically can significantly reduce the time needed to compute the map.

The other important tool is the Schwarz reflection principle, which states that if an analytic function extended to a straight or circular boundary arc maps this boundary to another straight or circular arc, then this function can be continued analytically across the arc by reflection.

2.1 Single Slit

The map to the single slit is composed of two separate stages. The first, appearing in an article by Szegő [24] (who attributes it to Schwarz), maps the interior of the ellipse E_ρ to the unit disk by

$$h_1(z) = \sqrt[4]{m}\,\mathrm{sn}\left(\frac{2K}{\pi}\arcsin(z)|m\right), \tag{2.3}$$

where $\mathrm{sn}(\cdot|m)$ is the Jacobi elliptic sine function [1, (16.1.5)] with parameter $m \in (0,1)$. This map sends the interval $[-1,1]$ to $[-m^{1/4}, m^{1/4}]$, and the ellipse parameter is related to m by

$$\rho = \exp\left(\frac{\pi K'(m)}{4K(m)}\right), \tag{2.4}$$

where $K(m)$ and $K'(m)$ are complete elliptic integrals of the first and second kind respectively [1, (16.1.1)]. Figure 2 shows h_1 as a further composition of simpler maps.

The second stage of the map sends the unit disk to the slit plane (2.1) with $[-m^{1/4}, m^{1/4}]$ mapping to $[-1,1]$. Since the boundary of $S_{\delta+i\varepsilon}$ describes a polygon (with vertices at infinity) we may use the Schwarz–Christoffel formula (2.2), and by symmetry the vertices, prevertices, and interior angles in the map can be taken to be

$$\begin{array}{lll} w_1 = \delta + i\varepsilon, & z_1 = \exp(i\theta), & \alpha_1 = 2, \\ w_2 = \infty, & z_2 = -1, & \alpha_2 = -1, \\ w_3 = \overline{w}_1, & z_3 = \overline{z}_1, & \alpha_3 = 2, \\ w_4 = \infty, & z_4 = 1, & \alpha_4 = -1. \end{array} \tag{2.5}$$

Substituting this information into (2.2), the map from the unit disk to the single conjugate slit plane can be written in the form

$$h_2(z) = A + C\int^z \left(\frac{(1-z_1)(1-\overline{z}_1)}{4(\xi-1)^2} + \frac{(1+z_1)(1+\overline{z}_1)}{4(\xi+1)^2}\right) d\xi. \tag{2.6}$$

Integrating (2.6) exactly, and noting that $z_1\overline{z}_1 = 1, z_1 + \overline{z}_1 = 2\cos(\theta)$, we find

$$h_2(z) = A - C\left(\frac{1-\cos(\theta)}{2(z-1)} + \frac{1+\cos(\theta)}{2(z+1)}\right), \tag{2.7}$$

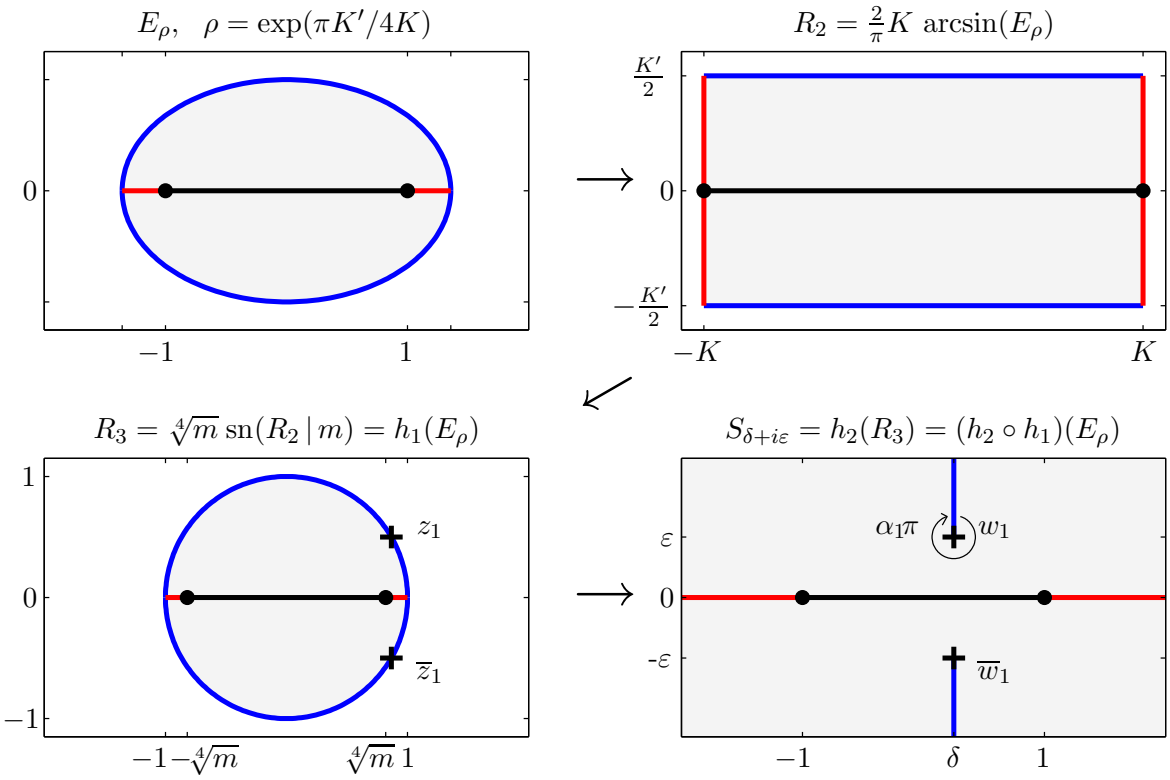

Figure 2: The conformal map $g = h_2 \circ h_1$ from the ellipse E_ρ to the single slit plane $S_{\delta+i\varepsilon}$ decomposed into a sequence of maps. The first three panels show Szegő's map (2.3) from the ellipse to the unit disk, where the principal operations are arcsin and the Jacobi elliptic function *sn*. The map from the disk R_3 to $S_{\delta+i\varepsilon}$ is given by the Schwarz–Christoffel formula (2.2).

where the four real unknowns A, C, θ and m are determined by the four real conditions $h_2(\pm m^{1/4}) = \pm 1$, $\mathrm{Re}\,(h_2(z_1)) = \delta$, and $\mathrm{Im}\,(h_2(z_1)) = \varepsilon$. Solving this system leads to

$$\cos(\theta) = \mathrm{sign}(\delta)\sqrt{\frac{(\delta^2+\varepsilon^2+1) - \sqrt{(\delta^2+\varepsilon^2+1)^2 - 4\delta^2}}{2}}, \tag{2.8}$$

$$m^{1/4} = \frac{-\varepsilon + \sqrt{\varepsilon^2 + \sin^2(\theta)}}{\sin(\theta)}, \tag{2.9}$$

$$A = \frac{\cos(\theta)}{m^{1/4}}, \quad C = \frac{1-\sqrt{m}}{m^{1/4}}. \tag{2.10}$$

Thus the conformal map $g = h_2 \circ h_1$ maps the interior of the ellipse E_ρ to the slit plane $S_{\delta+i\varepsilon}$, with ρ related to δ and ε through (2.4), (2.8) and (2.9).

Theorem 1 *If $g = h_2 \circ h_1$ maps E_ρ to $S_{0+i\varepsilon}$, the ellipse parameter satisfies*

$$\rho - 1 \sim \frac{\pi^2}{4\log(4/\varepsilon)}, \quad \text{as } \varepsilon \to 0^+. \tag{2.11}$$

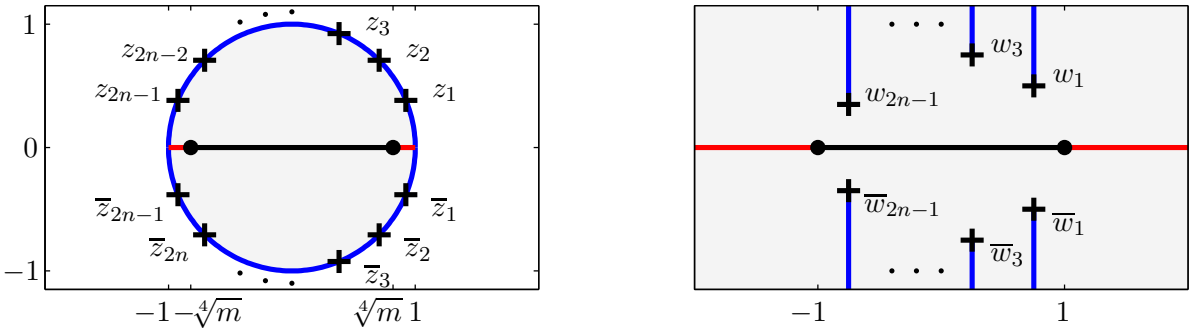

Figure 3: As in Figure 2c-d, but for the multiple slit map. The prevertices of the slits are located symmetrically with respect to the real axis around the unit disk and labelled in anti-clockwise order. The vertices of $S_{\{\delta_k+i\varepsilon_k\}_{k=1}^n}$ are labelled from right to left with the even-indexed vertices and their conjugates located at infinity.

Proof From (2.4) and the series expansion of the exponential we note that

$$\rho - 1 \sim \frac{\pi K'}{4K}, \quad \text{as } \frac{K'}{K} \to 0. \tag{2.12}$$

Using (2.8) and (2.9) one can show that $\sqrt[4]{m} = \sqrt{1+\varepsilon^2} - \varepsilon$, and ignoring powers of ε greater than one, we find that $1 - m \sim 4\varepsilon$ as $\varepsilon \to 0$. Next recall that $K' \sim \pi/2$ [1, (17.3.11)] and $K \sim \log(16/(1-m))/2$ [1, (17.3.26)] as $m \to 1$, or equivalently as $\varepsilon \to 0$, from which it follows that $K'/K \sim \pi/\log(4/\varepsilon)$ as $\varepsilon \to 0$. Substituting this into (2.12) gives the required result. ■

2.2 Multiple Slits

We now consider the more general case, allowing for multiple pairs of conjugate slits with n tips at $\{\delta_k \pm i\varepsilon_k\}_{k=1}^n$, and seek a map from the ellipse E_ρ to the region

$$S_{\{\delta_k+i\varepsilon_k\}_{k=1}^n} = \mathbb{C} \setminus \bigcup_{k=1}^{n} \{[\delta_k - i\varepsilon_k, \delta_k - i\infty] \cup [\delta_k + i\varepsilon_k, \delta_k + i\infty]\} \tag{2.13}$$

(Fig 3b). As before the map is considered in two stages: from the ellipse to the unit disk using (2.3), and then from this disk to the region $S_{\{\delta_k+i\varepsilon_k\}_{k=1}^n}$. Again this slit plane is a polygon, and substituting the interior angles and symmetry of the prevertices into the Schwarz–Christoffel formula (2.2) we find the map from the disk to the n-slit plane (2.13) can be expressed as

$$h_3(z) = A + C \int^z \frac{(\xi - z_1)(\xi - \overline{z}_1)}{(\xi-1)^2(\xi+1)^2} \prod_{k=1}^{n-1} \frac{(\xi - z_{2k+1})(\xi - \overline{z}_{2k+1})}{(\xi - z_{2k})(\xi - \overline{z}_{2k})} d\xi. \tag{2.14}$$

This can then be rewritten in partial fraction form as

$$h_3(z) = A + C\int^z \left(\frac{a_0}{(\xi-1)^2} + \frac{b_0}{(\xi+1)^2} + i\sum_{k=1}^{n-1} a_k \left(\frac{1}{\xi - z_{2k}} - \frac{1}{\xi - \overline{z}_{2k}} \right) \right) d\xi, \quad (2.15)$$

where the coefficients of the partial fraction expansion in the integrand are

$$a_0 = \frac{\prod_{j=0}^{n-1} \big(1 - \cos(\theta_{2j+1})\big)}{2\prod_{j=1}^{n-1} \big(1 - \cos(\theta_{2j})\big)}, \quad b_0 = \frac{\prod_{j=0}^{n-1} \big(1 + \cos(\theta_{2j+1})\big)}{2\prod_{j=1}^{n-1} \big(1 + \cos(\theta_{2j})\big)}, \quad (2.16)$$

$$a_k = \frac{\prod_{j=0}^{n-1} \big(\cos(\theta_{2k}) - \cos(\theta_{2j+1})\big)}{2\sin^3(\theta_{2k}) \prod_{\substack{j=1 \\ j\neq k}}^{n-1} \big(\cos(\theta_{2k}) - \cos(\theta_{2j})\big)}, \quad k = 1, 2, \ldots, n-1. \quad (2.17)$$

Thus integrating (2.15) exactly gives

$$h_3(z) = A + C\left(\frac{-a_0}{z-1} + \frac{-b_0}{z+1} + i\sum_{k=1}^{n-1} a_k \left(\log(z - z_{2k}) - \log(z - \overline{z}_{2k}) \right) \right), \quad (2.18)$$

where the $2n+2$ real unknowns A, C, $\theta_1, \theta_2, \ldots, \theta_{2n-1}$, and m can be determined from the $2n+2$ real conditions

$$\begin{aligned} h_3(\pm m^{1/4}) &= \pm 1, \\ \mathrm{Re}(h_3(z_{2k-1})) &= \delta_k, \quad k = 1, 2, \ldots, n, \\ \mathrm{Im}(h_3(z_{2k-1})) &= \varepsilon_k, \quad k = 1, 2, \ldots, n. \end{aligned} \quad (2.19)$$

In solving this parameter problem, we suggest that rather than considering all of the prevertices $\{z_k\}_{k=1}^{2n-1}$ amongst the unknowns (or more precisely their corresponding real-valued arguments $\{\theta_k\}$), a more efficient approach arises in considering (2.18) with the $2n+2$ real parameters $A, b_0, a_0, \ldots, a_{n-1}, \theta_2, \theta_4, \ldots, \theta_{2n-2}$ and m. In doing so, the system (2.19) separates into a linear system in the $n+2$ unknowns $A, b_0, \{a_k\}_{k=0}^{n-1}$ and a smaller nonlinear system in the n unknowns $\{\theta_{2k}\}_{k=1}^{n-1}$ and m [1]. To see this, suppose the latter n parameters have been chosen and observe that as z passes anticlockwise through z_{2k} on the upper half of the unit circle, the k^{th} term in the summation on the right-hand side of (2.18) causes a jump of $a_k\pi$ in the real part of h_3. The actual jump required is the horizontal distance to the next slit tip, and thus choosing $a_k = (d_{k+1} - d_k)/\pi$ will give exactly this spacing. Solving a simple 3×3 linear system then ensures that A, a_0, b_0 are chosen so that $h(\pm m^{1/4}) = \pm 1$ and $Re(h_3(z_1)) = \delta_1$.

This leaves a nonlinear system in the n unknowns $\{\theta_{2k}\}_{k=1}^{n-1}$ and m to determine the vertical distance of the n slit tips from the real line. The unknowns $\{\theta_{2k}\}$ are subject to

[1] The separation of a nonlinear problem as described above forms the basis of the Variable Projection method of Golub and Pereyra, and the corresponding FORTRAN routine VARPRO [15] developed some 30 years ago. A recent review by the original authors can be found in [14], where the better conditioning and faster convergence of the reduced problems are demonstrated.

strict inequality constraints $0 < \theta_2 < \theta_4 < \ldots < \theta_{2n-2} < \pi$, but these can be eliminated by transforming to an unconstrained set of variables

$$\phi_k = \arcsin\left(2\left(\frac{\theta_{2k} - \theta_{2k-2}}{\theta_{2k+2} - \theta_{2k-2}}\right) - 1\right), \quad k = 1, 2, \ldots, n-1, \tag{2.20}$$

where $\theta_0 = 0, \theta_{2n} = \pi$. The new variables take arbitrary real values, and the $\{\theta_{2k}\}$ can be recovered by solving the system of linear equations

$$\left(\frac{1 - \sin(\phi_k)}{2}\right)\theta_{2k-2} - \theta_{2k} + \left(\frac{1 + \sin(\phi_k)}{2}\right)\theta_{2k+2} = 0, \quad k = 1, 2, \ldots, n-1. \tag{2.21}$$

A similar transformation can be used to eliminate the constraint on m.

To solve the nonlinear system (2.19c), we require the positions of the slit tips $h_3(z_{2k-1})$, but locating these by computing the preimages $\{z_{2k-1}\}$ from (2.16)-(2.17) at first seems cumbersome. However, we simply note these points are the zeros of the integrand in (2.14) and furthermore that on the unit circle between the poles $\{z_{2k}\}$ the integrand is monotonic, allowing the single root between each two consecutive poles to be located by a simple algorithm combining Newton iteration and bisection. The system (2.19) can then be solved using any nonlinear system solver, such as the MATLAB routine `fsolve`, although we choose to use the freely available Newton–Armijo solver implemented in the routine `nsold` by Kelley [19]. We have found that the treatment of the parameters in this separable form allows faster and more robust solution of the parameter problem than by considering $\{\theta_k\}_{k=1}^{2n}$ as the unknowns directly.

Once the parameter problem is solved, h_1 can be computed (with ρ related to m as in (2.4)), and the map from the ellipse E_ρ to the multiply slit domain $S_{\{\delta_k + i\varepsilon_k\}_{k=1}^n}$ is given by $g = h_3 \circ h_1$. To evaluate this numerically, we require a means of computing the complete elliptic integrals $K(m), K'(m)$ and the Jacobi elliptic functions $\mathrm{sn}(\cdot|m), \mathrm{cn}(\cdot|m), \mathrm{dn}(\cdot|m)$. For real arguments these may be computed with the standard MATLAB routines `ellipke` and `ellipj` respectively. For complex arguments the elliptic functions can be computed via `ellipjc` from Driscoll's Schwarz–Christoffel Toolbox [10], which uses an algorithm based on the descending Landen transformation [1, (16.12)]. The MATLAB code below evaluates the map using these routines, although due to space constraints we omit the code necessary to form and solve the system of nonlinear equations to determine `z2k`$=\{z_{2k}\}_{k=1}^{n-1}$ and `m`$=m$ [2]. Additionally, we find in practice that the elliptic parameter m can often be very close to 1, making it beneficial to use the ascending Landen transform [1, (16.14)] with the complementary parameter $m_1 = 1 - m$ (which can be better represented in IEEE arithmetic).

```
m14 = m^(.25);                          % 4th root of elliptic paramter
L = -.5*log(m)/pi;
```

[2] A full code for computing the map to a multiply slit region appears in [26], although without taking advantage of the linear and nonlinear separation. For a general outline of methods for solving parameter problems in Schwarz–Christoffel maps, see [11, Chapter 3.1].

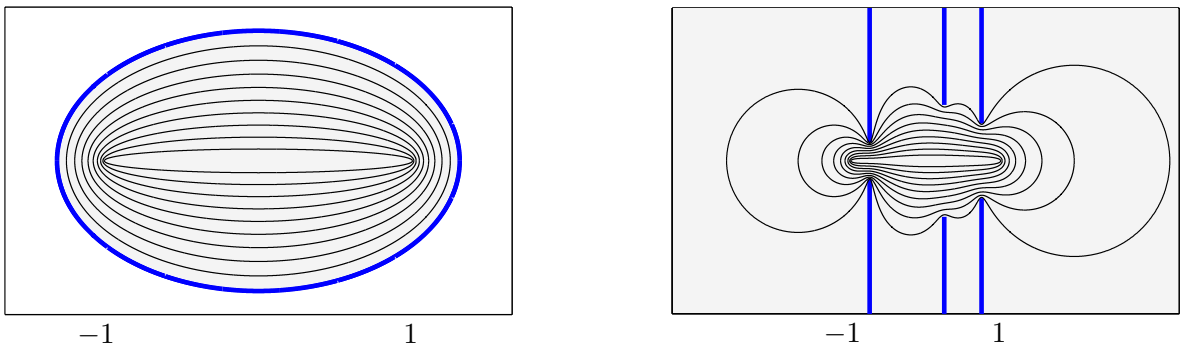

Figure 4: The image of the ellipse $E_{\exp(\pi K'/4K)}$ and smaller ellipses $E_{\exp(j\pi K'/40K)}, j = 1, \ldots, 9$ under the maps (2.3) and (2.18) to $S_{(3+2i,1+3i,-3+i)/4}$. If the assumption on the analyticity of f is incorrect, but f is analytic within say the largest region on the right, then convergence of the numerical method based on this map would be only 10% less than had the assumption been correct. The second largest region corresponds to 20% less, and so on.

```
[K Kp] = ellipkkp(L);                    % elliptic integrals
h1 = m14*ellipjc(2*K*asin(z(:))/pi,L); % the map to the disk (2.3)

% evaluate the summation on the rhs of (2.18)
ZZ = repmat([-m14;m14;h1],1,n-1);   Z2K = repmat(z2k.',length(h1)+2,1);
ZZ1 = ZZ - Z2K;                     idx1 = find(real(ZZ1)<0 & imag(ZZ1)>=0);
WW1 = log(ZZ1);                     WW1(idx1) = WW1(idx1) - 2i*pi;
ZZ2 = ZZ - conj(Z2K);               idx2 = find(real(ZZ2)<0 & imag(ZZ2)<0);
WW2 = log(ZZ2);                     WW2(idx2) = WW2(idx2) + 2i*pi;
ak = diff(d)/pi;                       % ak given by jumps in delta
sumlogs = 1i*((WW1 - WW2)*ak);         % the summation

% system of equations for A, a0, b0
M = (1-m14)^2/(4*m14); M = [2/(m14^2-1) .5 .5 ; -1 -M 1+M ; 1 -1-M M];
rhs = [ak'*(angle(z2k)-pi)+d(1) ; [-1;1]-sumlogs(1:2)];
lhs = -(1-m14^2)/(1+m14^2)*(M*rhs);
A = lhs(1); a0 = lhs(2); b0 = lhs(3);

g = A + a0./(h1-1) + b0./(h1+1) + sumlogs(3:end); % the map g(z) = h3(h1(z))
```

For example, in mapping to the region with slits at $(3 + 2i, 1 + 3i, -3 + i)/4$ we find;

```
m   =  0.523231225073770;
z2k = [0.830135290736502 + 0.557562013657515i
       0.221599693267731 + 0.975137721526374i];
```

and substituting these values to the code above, we plot in Figure 4 the image of the ellipse E_ρ with $\rho = \pi K'(m)/4K(m)$, as well as the images of the smaller ellipses where $\rho \mapsto \rho^{j/10}, j = 1, \ldots, 9$.

3 Periodic Strips to Periodic Infinite Slits

If the fundamental region for methods based upon algebraic polynomial approximation is the ellipse with foci at ± 1, the corresponding region for trigonometric polynomial approximation is an infinite strip about the real axis. For example, when a 2π-periodic function f can be continued analytically to the closed strip of half-height η, the Fourier spectral method with N collocation points approximates f' on $[-\pi, \pi]$ with an error that decays at a rate $O(e^{-\eta N})$ as $N \to \infty$ [25]. A similar result governs convergence of the trapezium rule applied to 2π-periodic analytic functions [8], and such results are a consequence of the exponential decay of coefficients in the Fourier expansion of f [7, Chapter 2.10].

If we assume as before, that a function f is analytic in each 2π-periodic vertical strip excluding one or more pairs of conjugate slits extending to infinity, then to enlarge the region of analyticity we seek a 2π-periodic map g from the infinite strip Σ_η of half-height η to such a slit plane. We derive this map first to the region

$$\mathcal{S}_{\delta+i\varepsilon} = \mathbb{C} \setminus \bigcup_{j=-\infty}^{\infty} [(\delta + 2j\pi) \pm i\varepsilon, (\delta + 2j\pi) \pm i\infty], \quad \varepsilon > 0, \tag{3.1}$$

with just one pair of slits in each period (Fig 5b), before generalising to allow an arbitrary number of slits (Figure 5c). Rates of convergence can then be improved by applying the numerical methods to the 2π-periodic function $f \circ g$, or by using g to define a linear trigonometric rational interpolant [2] (see §4 for more detail).

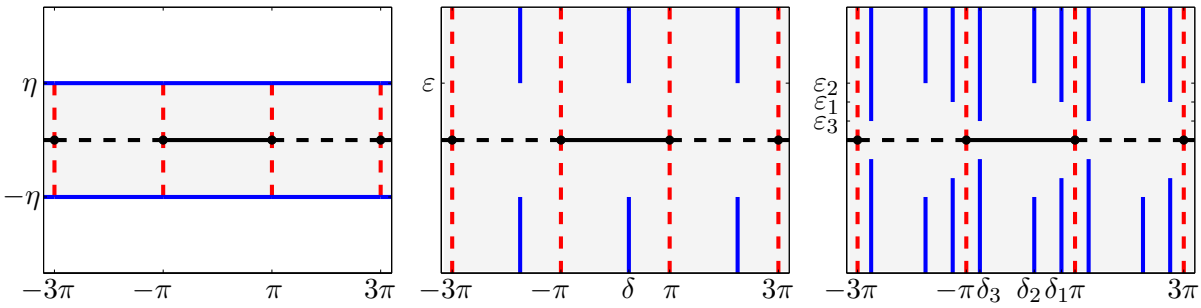

Figure 5: The maps of §3. In §3.1 we derive a map from the infinite strip Σ_η (left) to the single periodic slit plane $\mathcal{S}_{\delta+i\varepsilon}$ (centre) which preserves intervals on the real line of width 2π. In §3.2 we re-derive this using a different approach, which is then generalised to produce a map from Σ_η to a multiple periodic slit plane, such as $\mathcal{S}_{\{\delta_k+i\varepsilon_k\}_{k=1}^3}$ (right).

3.1 Single Slit

The periodic map from the strip Σ_η to the single periodic slit plane $\mathcal{S}_{\delta+i\varepsilon}$ can be derived directly using a sequence of elementary maps, and by repeated application of the Schwarz

reflection principle, the problem reduces to mapping the interior of a rectangle R_1 of width π and height

$$\eta = \frac{\pi K'}{K} \tag{3.2}$$

to a semi-infinite strip R_4 (Figure 6). The first map in the sequence rescales R_1 to a width K and height K', which the Jacobi elliptic function $\mathrm{sn}^2(z|m)$ maps to the upper-half plane R_2 when $K = K(m)$ and $K' = K'(m)$ are complete elliptic integrals of parameter m [20, (13.2)]. The upper-half plane is then mapped to itself by the Möbius transformation

$$z \mapsto \frac{(1-m)z}{1-mz}, \tag{3.3}$$

before a square root takes this to the upper-right quadrant R_3. Observing $\sin(z/2)$ maps the semi-infinite strip R_4 to R_3 [20, (10.5)], we use the inverse of this to map to R_4. Combining the above, reflecting across $\mathrm{Re}(z) = 0$ and translating in the real direction by a distance δ, the 2π-periodic map from Σ_η to $\mathcal{S}_{\delta+i\varepsilon}$ is

$$g(z) = \delta + 2\arcsin\left(\sqrt{\frac{(1-m)\mathrm{sn}^2(\frac{K}{\pi}z|m)}{1-m\mathrm{sn}^2(\frac{K}{\pi}z|m)}}\right), \tag{3.4}$$

where the elliptic parameter m is related to ε by

$$m = \mathrm{sech}^2(\varepsilon/2), \tag{3.5}$$

and the height η of the strip is given by substituting the complete elliptic integrals $K(m)$ and $K'(m)$ into (3.2). Noting that $\mathrm{sn}^2(\frac{K}{\pi}(z+2\pi)|m) = \mathrm{sn}^2(\frac{K}{\pi}z|m)$ [1, (16.8.1)], it is clear that g is 2π-periodic, although we have not enforced that (3.4) satisfies $g(\pm\pi) = \pm\pi$. However, as the boundary of the map is invariant under a horizontal translation of R_1 this can be achieved by replacing z by $(z + g^{-1}(\pi) - \pi)$ in the right-hand side of (3.4) if required.

Theorem 2 *The half-height η of the strip mapped to $\mathcal{S}_{\delta+i\varepsilon}$ by (3.4) satisfies*

$$\eta \sim \frac{\pi^2}{2\log(8/\varepsilon)}, \quad \text{as } \varepsilon \to 0^+. \tag{3.6}$$

Proof Recall from Theorem 1 that $K' \sim \pi/2$ and $K \sim \log(16/(1-m))/2$ as $m \to 1$, which substituted into (3.2) implies

$$\eta \sim \frac{\pi^2}{\log\left(16/(1-m)\right)}, \quad \text{as } m \to 1. \tag{3.7}$$

From the asymptotic expansion of (3.5) for small ε, one can show that $1 - m \sim \varepsilon^2/4$ as $\varepsilon \to 0$, which combined with the above gives the result required. ■

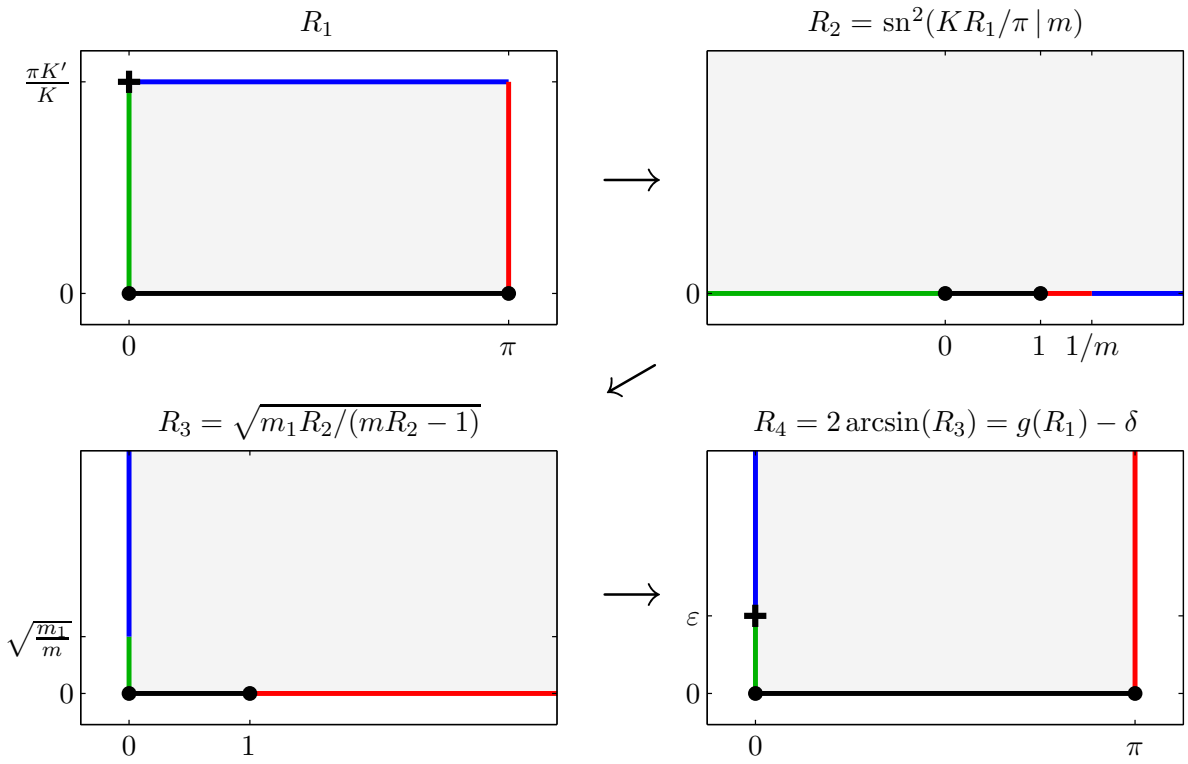

Figure 6: The separate stages of the map g from a periodic rectangle of half-height η to the the periodic plane with slits at $2j\pi + i\varepsilon, j = 0, \pm 1, \ldots$. It is interesting to note that as with the map shown in Figure 2, the key operations are arcsin and sn, only here the order in which they are applied is reversed.

3.2 Multiple Slits

We next consider the map to a region with multiple slits removed from each periodic interval, which we denote by

$$\mathcal{S}_{\{\delta_k + i\varepsilon_k\}_{k=1}^n} = \mathbb{C} \setminus \left\{ \bigcup_{j=-\infty}^{\infty} \bigcup_{k=1}^{n} [(\delta_k + 2j\pi) \pm i\varepsilon_k, (\delta_k + 2j\pi) \pm i\infty] \right\}. \tag{3.8}$$

The Schwarz–Christoffel formula for a periodic map from a strip to a general polygon can be found in [11, 13], but the situation here is simplified as the interior angles of $\mathcal{S}_{\{\delta_k + i\varepsilon_k\}}$ are integer multiples of π; 2π at the tip of a slit, 0 at infinity and π on the real axis. By symmetry we need only consider mapping the upper half of Σ_η to the upper half of $\mathcal{S}_{\{\delta_k + i\varepsilon_k\}_{k=1}^n}$, and the Schwarz–Christoffel map to an n-slit region is given by

$$h(z) = A + C \int^z \prod_{j=-\infty}^{\infty} \prod_{k=1}^{n} \frac{\sinh \frac{\pi}{2}(\xi - z_{2k} - jT)}{\sinh \frac{\pi}{2}(\xi - z_{2k-1} - jT)} d\xi, \tag{3.9}$$

where the period T of the vertices is unknown and must be determined as part of the solution. However, the infinite product makes the integral in this representation difficult

to manipulate analytically, and evaluating it numerically when solving the parameter problem is computationally expensive. In order to proceed, we take a different approach.

Recall the foundation of the Schwarz–Christoffel transformation is that the derivative of the map $g : \mathcal{D} \to \mathcal{P}$ can be expressed as a product $g' = \prod g_k$ of canonical functions g_k, which have piecewise constant argument along $\partial\mathcal{D}$ [11, Chapter 2]. When this is the case, g is piecewise linear along the boundary and thus maps $\mathcal{D}$ to the interior of a polygon. If $\mathcal{D}$ is also a polygon and the jumps in argument of g' occur at prevertices $z = z_k$ where $\partial\mathcal{D}$ has an interior angle $\beta_k\pi$, then $\mathcal{P}$ will have corners at $w_k = g(z_k)$ with interior angles

$$\alpha_k\pi = \beta_k\pi - [\arg g']_{z_k^-}^{z_k^+}. \tag{3.10}$$

We propose to recompute the map to a single-slit region using an idea based upon these facts, i.e. find a function g' piecewise constant along the boundary of the periodic strip with jumps in argument that lead to angles which create a slit domain.

Neglecting one of the symmetry arguments in the previous derivation that will not be applicable in the multiply slit case to follow, we take as our initial domain R_1 the rectangle $[-\pi, \pi] \times [0, \eta]$. This is then scaled by K/π to give

$$R_2 = [-K, K] \times [0, iK'], \tag{3.11}$$

where as usual K and K' are complete elliptic integrals, and are related to η by (3.2). Figure 7 shows how the third Jacobi elliptic function $\mathrm{dn}(z|m)$ has piecewise constant argument on the boundary of R_2 [20, p.176]. The interval $[K, -K] + iK'$ is mapped periodically by dn to the imaginary axis, with $\mathrm{dn}((2j+1)K+iK'|m) = 0$ and $\mathrm{dn}(2jK+iK|m) = \infty$ for all integers j [1, (16.2,16.8.3,16.5)]. Travelling from right to left, the argument of $\mathrm{dn}(z = z_R + iK'|m)$ jumps by $-\pi$ on either side of $z_R = (2j+1)K$ and by π across $z_R = 2jK$. Substituting these jumps to (3.10), we find the interior angles of $\mathrm{dn}(\partial R_2|m)$ at these points are 2π and 0. Thus it follows that a map of the form

$$h_4(z) = A + C\int^z \mathrm{dn}(\xi|m)d\xi \tag{3.12}$$

must periodically map the boundary ∂R_2 to a slit region, where $h((2j+1)K + iK')$ and $h(2jK + iK'), j = 0, \pm1, \ldots$ are the tips of slits and points at infinity respectively. The lower edges of the rectangle $[-K, 0], [0, K]$ are mapped by dn to $[m_1^{1/2}, 1], [1, m_1^{1/2}]$ so that $h_4([-K, K])$ is a real interval, and one can also show the vertical lines $\pm K + [0, iK']$ are mapped by dn to the real axis [1, (16.8.3,16.20.3)], therefore connecting the slit tips to the real axis under h_4 as shown in Figure 7(bottom left).

There are two further steps to complete the map (3.12) to $\mathcal{S}_{0+i\varepsilon}$; to find an explicit expression for h_4 by integrating the elliptic function $\mathrm{dn}(\cdot|m)$, and to solve the parameter problem to ensure the tip of the slit is positioned correctly and repeated with the correct period. For $x \in R_2$ the integral of dn is [1, (16.24.3)]

$$\int^x \mathrm{dn}(\xi|m)d\xi = \arcsin(\mathrm{sn}(x|m)), \tag{3.13}$$

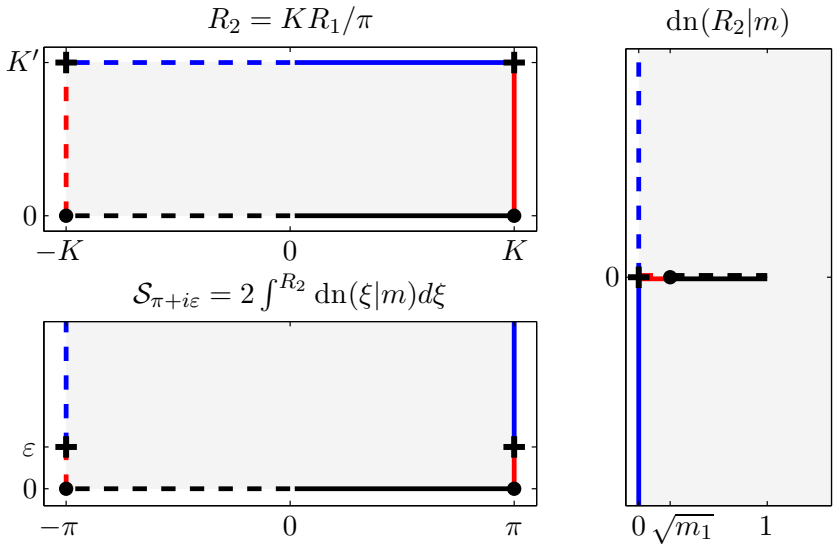

Figure 7: The rectangle R_2 (top left) is mapped to the right half-plane by the elliptic function $dn(\cdot|m)$ (right); in particular the top boundary is mapped to the imaginary axis. By considering the jumps in argument of this function along the boundary of R_2, we show its integral h_4 maps to the slit region $\mathcal{S}_{\pi+i\varepsilon}$ (bottom left). The key in constructing maps to multiple slit regions is that a positive linear combination of shifted elliptic functions will map to the same region on the right (see Figure 8).

which is sometimes referred to as the *amplitude* $\mathrm{am}(x|m)$ [1, (16.1.4)]. Writing $z = x + 2N_zK : x \in R_2$ we find

$$\begin{aligned} \int^z \mathrm{dn}(\xi|m)d\xi &= \int^x \mathrm{dn}(\xi|m)d\xi + \sum_{j=1}^{N_z} \int_{x+2(j-1)K}^{x+2jK} \mathrm{dn}(\xi|m)d\xi \\ &= \arcsin(\mathrm{sn}(x|m)) + N_z\pi. \end{aligned} \tag{3.14}$$

Thus allowing for scaling and horizontal translation, the map h_4 takes the form

$$h_4(z = x + 2N_zK : x \in R_2) = A + C(\arcsin(\mathrm{sn}(x|m)) + N_z\pi), \tag{3.15}$$

where the unknown real parameters A, C and m are determined by the three real conditions, $|h(K) - h(-K)| = 2\pi, h(K + iK') = i\varepsilon$. Solving this system, the map $g(z) = \delta + h_4(\frac{K}{\pi}z)$ from Σ_η to $\mathcal{S}_{\delta+i\varepsilon}$ is given by

$$g(z) = \delta + (2N_z + 1)\pi + 2\arcsin\left(\mathrm{sn}\left(Kx/\pi|m\right)\right), \tag{3.16}$$

where

$$z = x + 2N_z\pi : x \in R_2 \cup \overline{R}_2 \tag{3.17}$$

and as before $m = \mathrm{sech}^2(\varepsilon/2)$ is related to η by (3.2). Again it is not enforced that $g(\pm\pi) = \pm\pi$, but this can be achieved by a horizontal translation of z in the right-hand side of (3.16) (with x and N_z adjusted appropriately). In particular, shifting $z \mapsto z + K(m)$ we find that (3.16) reproduces (3.4).

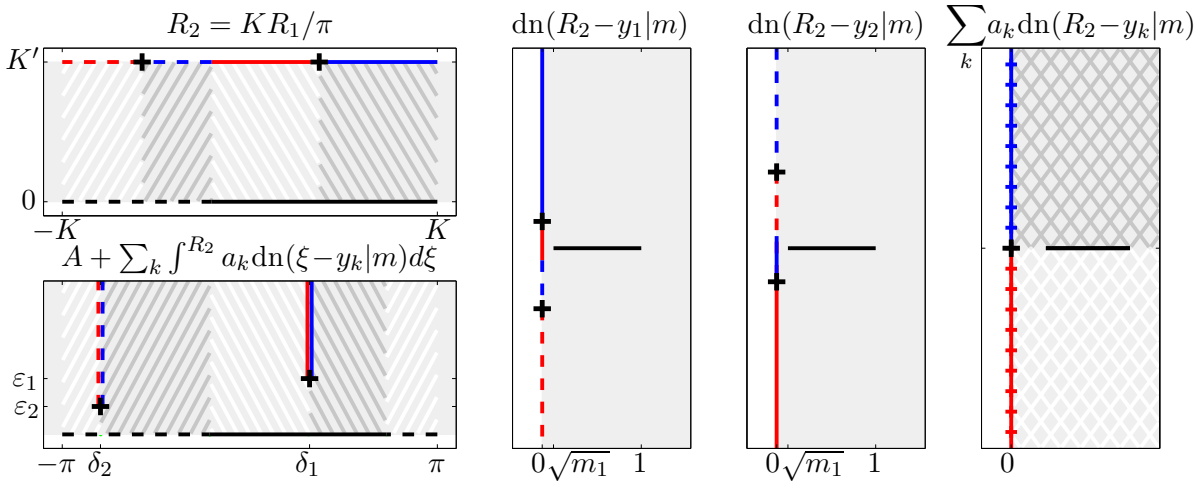

Figure 8: The upper boundary of the rectangle R_2 (top left) is mapped to the imaginary axis by each of the shifted elliptic functions $\mathrm{dn}(z - y_1|m)$ and $\mathrm{dn}(z - y_2|m)$ (centre), and any positive linear combination of these two functions will also map to the imaginary axis (right). As in Figure 7, the interior angles of this sum satisfy (3.10) so that its integral maps to a slit plane (bottom left), where the preimages of the slit tips are the roots of the integrand.

We now extend the idea used above to the situation of a multiply slit target region. The key observation is that for any $y_k \in \mathbb{R}$, the shifted elliptic functions $\mathrm{dn}(z - y_k|m)$ will each be $2K(m)$-periodic in the real direction and map $[K, -K] + iK'$ to the imaginary axis. Furthermore, the linear combination

$$h_5'(z) = \sum_{k=1}^{n} a_k \mathrm{dn}(z - y_k|m), \quad \{a_k > 0\} \tag{3.18}$$

will have these same properties for any $\{a_k > 0\}$ (Figure 8). Now, as before, traversing the upper boundary of ∂R_2 from right to left, the argument under h_5' jumps by $-\pi$ and π each time we cross a root or pole respectively, and substituting these jumps to (3.10) we find that

$$h_5(z) = A + \sum_{k=1}^{n} a_k \int^{z} \mathrm{dn}(\xi - y_k|m) d\xi \tag{3.19}$$

periodically maps the strip Σ_η to a multiply slit region (with n slits). We can express h_5 explicitly by writing $(z - y_k) = x_k + 2N_{z,k}K$ where $x_k \in R_2$ and applying (3.14) to give

$$h_5(z) = A + \sum_{k=1}^{n} a_k (\arcsin(\mathrm{sn}(x_k|m)) + N_{z,k}) \quad : x_k = (z - y_k) - 2N_{z,k}K \in R_2. \tag{3.20}$$

It then just remains to find parameters $A, \{a_k\}_{k=1}^n, \{y_k\}_{k=1}^n$ and m so that the slit tips are positioned at $\{\delta_k + i\varepsilon_k\}_{k=1}^n$.

Since the boundary of the slit map will not change under horizontal translation of R_1, one of the y_k is arbitrary and we assume without loss of generality that

$$K = y_1 > y_2 > \ldots > y_n > -K. \tag{3.21}$$

If $\{z_k\}_{k=1}^n$ are the preimages of the slit tips given by h_5, the remaining $2n+1$ free parameters are chosen to match the $2n+1$ real conditions $h_5(z_k) = \delta_k + i\varepsilon_k, k = 1, \ldots, n$ and the period of the slit domain $|h_5(z_1) - h_5(z_1 + 2K)| = 2\pi$. In the form (3.20) there seems no obvious way to explicitly relate these points $\{z_k\}$ to the shifts $\{y_k\}$ and coefficients $\{a_k\}$. The preimages of the points at infinity present no problem, since they are the poles of h_5' which are in turn the poles $(y_k + 2jK) + iK', j = 0, \pm 1, \pm 2, \ldots, k = 1, \ldots, n$ of $\mathrm{dn}(z - y_k|m)$. However, the prevertices of the slit tips are the zeros of h_5' (where the jumps take place) which lie along the line $\mathrm{Im} z = iK'$ between each of the poles, and can be computed with little difficulty in a similar way to the multiple slit map from the ellipse.

Furthermore, as in the previous section the parameter problem can be reduced to two weakly coupled linear and nonlinear components, each with $n+1$ and n parameters respectively. Since $\mathrm{Re}(\arcsin(\mathrm{sn}(z|m)))$ jumps at $z = iK'$ by a distance $-\pi$, $\mathrm{Re}(h(z))$ jumps at $z = y_k + iK'$ by a distance $-a_k\pi$ and

$$\begin{aligned} A &= \delta_1 - \pi, \\ a_k &= -(\delta_{k+1} - \delta_k)/\pi, \qquad k = 1, \ldots, n-1, \\ a_n &= -((\delta_1 - 2\pi) - \delta_n)/\pi, \end{aligned} \tag{3.22}$$

can be chosen instantly to match the position of the first slit, the correct distance between consecutive slits and a period of 2π. Thus the nonlinear system only needs to solve for the heights of the slits through the n parameters $\{y_k\}_{k=2}^n$ and m, which can be transformed to an unconstrained problem in a similar manner as in the previous section.

Again omitting the code to form and solve this nonlinear system to find the correct values for the parameters `yk` = $\{y_k\}_{k=1}^N$and `m` = m, the following MATLAB code computes the map $g = h_5(Kz/\pi)$ from Σ_η to $\mathcal{S}_{\{\mathtt{d(k)}+i\varepsilon_k\}_{k=1}^N}$.

```
L = -.5*log(m)/pi; [K Kp] = ellipkkp(L);  % elliptic integrals

ZZ = repmat(K*z(:).'/pi,length(yk),1);    % R2 (repeated)
YK = repmat(yk,1,length(z));              % yk (repeated)
ZZ1 = ZZ - YK;                            % z - yk
Nz = floor(.5*(real(ZZ1)/K+1));           % ZZ1 = X + 2*Nz*K : Re(X)\in[-K,K)
sn = ellipjc(ZZ1 - 2*Nz*K,L);             % elliptic function sn(X|m)
gk = asin(sn) + Nz*pi;                    % gk

A = d(1) - pi;                            % constant A
ak = -diff([d ; (d(1)-2*pi)])/pi;         % ak given by jumps in real part
g = A + gk.'*ak;                          % g = A + sum_k ak*gk
```

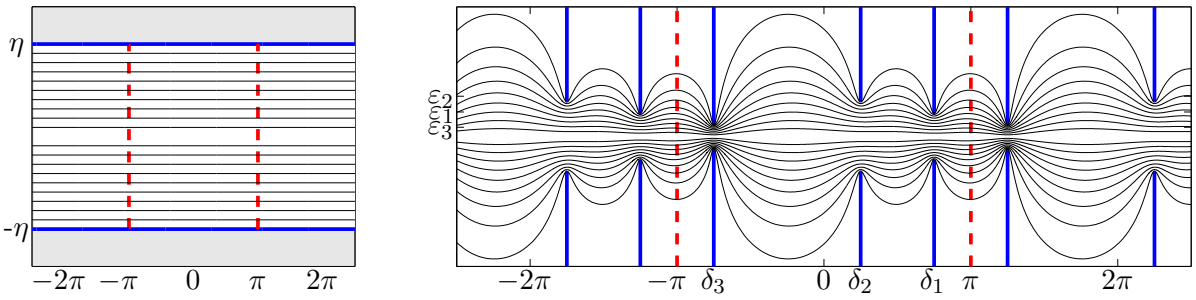

Figure 9: As in Fig 4, but here showing the images of the strips $\Sigma_{j\pi K'/10K}, j = 1, \ldots, 10$ (left, not to scale) under the map (3.20). As before, if the 2π-periodic function f is only analytic in the curved regions on the right, then the numerical method induced by g converges at a rate only $10\%, 20\%, \ldots$ slower than had f been analytic in $\mathcal{S}_{(3\pi+2i,\pi+3i,-3\pi+i)/4}$.

For example, in the map to the region with slits at $(3\pi+2i, \pi+3i, -3\pi+i)/4+2j\pi, j = 0, \pm1, \ldots$ we find

```
m  =  0.999620736713857;
yk = [5.325344471289760
      2.564368861260099
     -2.384269371859549];
```

which can be used to produce Figure 9.

4 Applications

We now demonstrate how the maps derived in this paper can be applied to spectral methods for solving differential equations, in particular those whose solutions u exhibit localised regions of rapid variation indicative of nearby singularities in the complex plane. One manner in which this might be achieved is to consider the map g as a change of variables, and apply the spectral method to approximate $u \circ g$ directly as in mapped-spectral methods [21]. The drawback of this approach however is that it requires both the tedious processes of rewriting the differential equation into new coordinates and of computing derivatives of the map. Instead we use g to define a linear rational interpolant [4]

$$r_N[g](x) = \frac{\sum_{k=0}^{N}{}'' \dfrac{(-1)^k}{x - g(x_k)} u(g(x_k))}{\sum_{k=0}^{N}{}'' \dfrac{(-1)^k}{x - g(x_k)}}, \quad x_k = -\cos(k\pi/N), \tag{4.1}$$

obtained by taking the usual barycentric weights for polynomial interpolation in Chebyshev points, but interpolating instead at the mapped Chebyshev points $g(x_k)$. This interpolant can be differentiated to form the basis of a linear rational collocation method

[3, 6], and the following theorem demonstrates the convergence the interpolant (4.1) and its derivatives:

Theorem 3 ([26]) *If $r_N[g]$ is the linear rational interpolant (4.1) defined by a conformal map g from a closed ellipse $\overline{E}_\rho$ in which $u \circ g$ is analytic, then*

$$r_N^{(n)}[g](x) - u^{(n)}(x) = O(\rho^{-N}), \quad \text{as } N \to \infty \tag{4.2}$$

for all $x \in [-1, 1]$ and all integers $n \geq 1$.

Experiments (both our own and those of [3]) show little difference between the mapped-polynomial and linear rational approaches in practice, although further investigation is certainly warranted. For periodic problems we use the spectral collocation method based upon the linear rational trigonometric interpolant [2], for which a similar theorem to the above holds.

4.1 Example 1

As our first example, we consider the ODE

$$\varepsilon \frac{d^2u}{dx^2} + x(x^2 - 1/2)\frac{du}{dx} + 3(x^2 - 1/2)u = 0, \quad -1 < x < 1, \quad \varepsilon > 0, \tag{4.3}$$

$$u(-1) = -2, \quad u(1) = 4.$$

This two-point boundary value problem appears in [22, Fig. 10.1], only above it has been differentiated so the solution u here is the derivative of the solution in [22]. The ODE has turning points at $x = 0, \pm 1/\sqrt{2}$, and u has interior layers at the latter two of these points [3]. We make an educated guess in choosing the conformal map by supposing u has singularities along the lines $\mathrm{Re} z = \pm 1/\sqrt{2}$, and, based upon the width of the interior layers, that the closest of these to the real axis are positioned at the four points

$$w = \pm 1/\sqrt{2} \pm i2.5\sqrt{\varepsilon}. \tag{4.4}$$

It is important to note that a crucial feature of the methodology we are suggesting is that it is not necessary to locate singularities to any great accuracy (as suggested by Figures 4 and 9), nor is it at all required that the solution have an particular singularity structure. The true solution might have a pole, a branch point, a string of poles, or perhaps be something like the error function, which is entire but grows so rapidly in the complex plane that it may be considered 'numerically singular'. To simplify exposition, we refer to the slit tips $\{\delta_k \pm i\varepsilon_k\}$ as if they were singularities of the solution u.

Solving the parameter problem for the map $g = h_3 \circ h_1$ from §2 for $\varepsilon = 10^{-5}$ with the assumptions (4.4), we find `m = 0.999526181050237` and `zk = i` (the latter is evident by

[3] It is suggested in [22] that the turning point at $x = 0$ might also cause 'turning point behaviour', and a grid highly clustered about this point is used. In our own computations we find this unnecessary, and map only to slits with real parts at $\pm 1/\sqrt{2}$ where the solution varies rapidly.

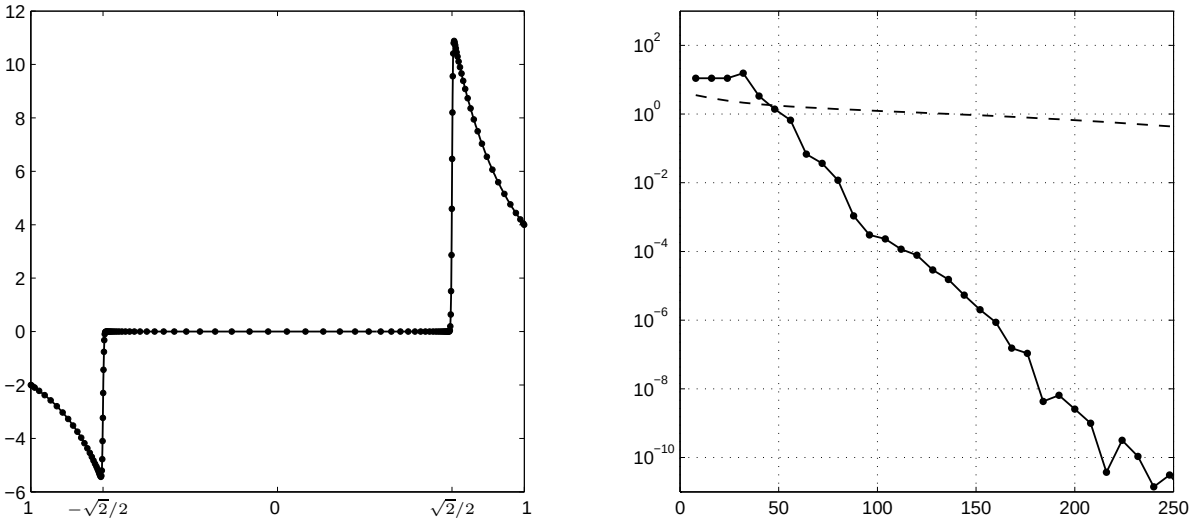

Figure 10: Left: An approximate solution to (4.3) with $\varepsilon = 10^{-5}$ obtained from the rational spectral method with 123 grid points (dots) defined by the map g. Right: the improvement in convergence of the transformed grid (solid) over the Chebyshev grid (dashed) as the number of collocation points $N + 1$ is increased. As the plot has a log-linear scale, straight lines represent geometric convergence.

symmetry), with which we can compute g and the differentiation matrices of the linear rational collocation method (concise MATLAB codes for computing these matrices can be found in [27]). Figure 10a shows this solution to (4.3) for $\varepsilon = 10^{-5}$ with 123 grid points (the same values as used in [22]), and Figure 10b compares the convergence of this approach against the standard Chebyshev method as the number of collocation points $N + 1$ increases.

4.2 Time-dependent problem

In general the locations of the singularities (or any singular-type behaviour) in the underlying solution are not known in advance. In [27] they are approximated on the fly using a Padé approximation technique, which is easily extended to the case of multiple singularities and periodic problems. The algorithm for this adaptive method for time-dependant problems is as follows.

Given a function u at collocation points $x_0^{(m)}, x_1^{(m)}, \ldots, x_N^{(m)}$ and time $t = t_m$:

1. Approximate the location of nearby singularities of u.

2. Adapt collocation points:
   compute the parameters of the map g with slit tips at these singularites,
   define $x_k^{(m+1)} = g(-\cos(k\pi/N)), \quad k = 0, \ldots, N.$

3. Advance in time:
   interpolate u to $\{x_k^{(m+1)}\}$,

construct new differentiation matrices given by g,
compute u at $t = t_{m+1}$ using time-stepping method.

For periodic problems the algorithm is unchanged other than using the periodic version of the slit map to adapt the equally spaced collocation points $(2k-N)\pi/N, k = 1\ldots, N$. The algorithm can also be modified to solve time-independent problems.

In the examples to follow, we discretise temporally by a highly accurate 7-stage, 13^{th}-order fully implicit Runge-Kutta RADAU IIA method with step size control [16]. Our MATLAB implementation uses coefficients from Hairer and Wanner's FORTRAN 77 subroutine RADAUP [17] and follows the structure of the MATLAB routine `radau5` written by Engstler [12]. We impose small relative and absolute error tolerances of 10^{-10} and 10^{-12} respectively so that the results are dominated by spatial rather than temporal errors. In practice one could use any time stepping routine which allows the option of pausing after each time step to adapt the grid points.

We consider a time-dependent Allen-Cahn equation, with initial and boundary conditions taken from [28, p34.m]:

$$\frac{\partial u}{\partial t} = \varepsilon \frac{\partial^2 u}{\partial x^2} + u(1-u^2), \quad -1 < x < 1, \quad t > 0, \tag{4.5}$$

$$u(x,0) = 0.53x + 0.47\sin(-1.5\pi x), \quad u(-1) = -1, u(1) = 1.$$

The solution u has stable equilibria at ± 1 and an unstable equilibrium at 0. Regions of the solution near ± 1 are flat, and the interfaces between these regions remain unchanged for an exponentially long time as a function of ε before changing abruptly, a phenomenon known as metastability. Figure 11 summarises the result of solving (4.5) using the adaptive spectral method for the parameter $\varepsilon = 10^{-4}$, which is 100 times smaller than that used in [28, p34.m].

4.3 Periodic time-dependant problem

As our final example, we consider the viscous Burgers' equation

$$\frac{\partial u}{\partial t} = \upsilon \frac{\partial^2 u}{\partial x^2} - u\frac{\partial u}{\partial x}, \quad -\pi < x < \pi, \quad t > 0, \quad \upsilon > 0, \tag{4.6}$$

with periodic initial and boundary conditions

$$u(x,0) = 0.5\cos(2x) - \sin(3x), \quad u(x,t) = u(x+2\pi,t). \tag{4.7}$$

As the problem is periodic, we use a conformal map of the form derived in §3 and a periodic implementation of the adaptive spectral method based upon the trigonometric linear rational interpolant [2]. Figure 12 shows the result of using this method to solve (4.6) with $\upsilon = 10^{-2}$. The initial solution quickly develops three steep fronts, which travel horizontally before ultimately smoothening out as time progresses. The singularities (or singular-type behaviour) nearby in the complex plane responsible for these fronts are tracked using a trigonometric version of the Padé approximation described in [27], and a

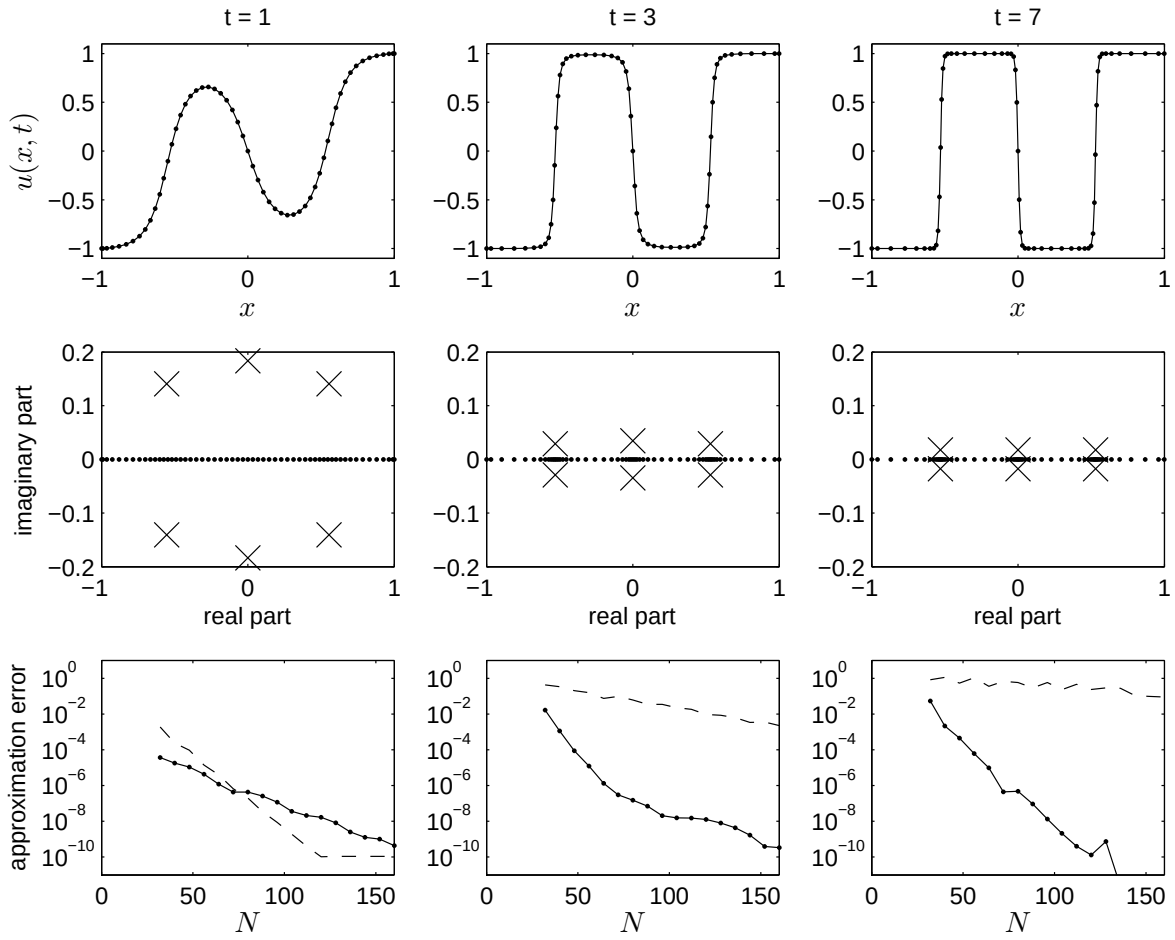

Figure 11: Solutions of the metastable problem (4.5) with $\varepsilon = 10^{-4}$ using the adaptive rational spectral method. The first row shows the solution computed using 57 collocation points (dots), whilst the second row shows the poles used in the corresponding computation (crosses). The third row shows log-linear plots of approximation error against the number of collocation points $N + 1$ for the rational adaptive (solid) and Chebyshev (dashed) spectral methods.

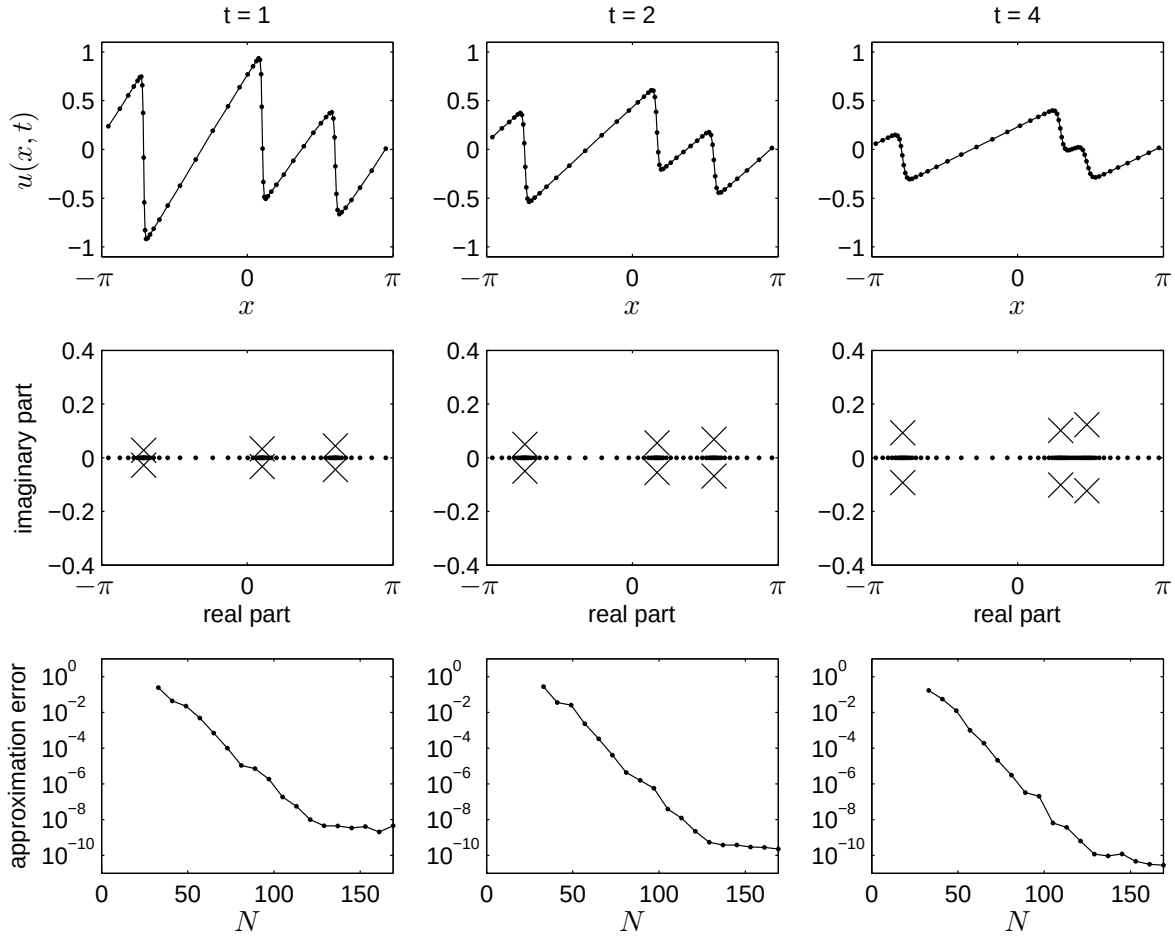

Figure 12: As Figure 11 but for Burgers' equation (4.6) with $\upsilon = 10^{-2}$ using the periodic map of §3 and the periodic implementation of the adaptive spectral method. The standard Fourier spectral method fails to obtain a solution with fewer than 280 collocation points, and even with $N = 512$ is accurate only to around 3 digits.

conformal map chosen appropriately. Using this technique we are able to find an accurate representation of the solution using relatively few collocation points, for example 3 digits of accuracy with around 50 points, whereas the standard Chebyshev method will not converge with fewer than 280 points. With 100 points one can obtain a solution accurate to around 8 or 9 digits, whilst the Chebyshev method with 512 points is accurate only to about 3 or 4.

Acknowledgments

We are grateful for the helpful suggestions of the Schwarz-Christoffel experts Toby Driscoll and Nick Trefethen, in particular to Nick for suggesting the separation of the nonlinear parameter problem in the multiple-slit maps and for his exceptional proof-reading abilities.

References

[1] Milton Abramowitz and Irene A. Stegun, *Handbook of Mathematical Functions with Formulas, Graphs, and Mathematical Tables*, Dover, New York, 1964.

[2] R. Baltensperger, *Some results on linear rational trigonometric interpolation*, Computers and Mathematics with Applications, 43 (2002), pp. 737–746(10).

[3] Richard Baltensperger and Jean-Paul Berrut, *The linear rational collocation method*, J. Comput. Appl. Math., 134 (2001), pp. 243–258.

[4] R. Baltensperger, J.-P. Berrut, and B. Noël, *Exponential convergence of a linear rational interpolant between transformed Chebyshev points*, Math. Comput., 68 (1999), pp. 1109–1120.

[5] Serge Bernstein, *Quelques remarques sur l'interpolation*, Journal Mathematische Annalen, 79 (1918), pp. 1–12.

[6] Jean-Paul Berrut and Richard Baltensperger, *The linear rational pseudospectral method for boundary value problems*, BIT Numerical Mathematics, 41 (2001), pp. 868–879(12).

[7] J. P. Boyd, *Chebyshev and Fourier spectral methods: Second Revised Edition*, Dover Publications, New York, 2001.

[8] P. J. Davis, *On the numerical integration of periodic analytic functions, in R. E. Langer, ed.*, On Numerical Integration: Proceedings of a Symposium, Madison, April 21–23, 1958, (1959), pp. 45–59.

[9] ——, *Interpolation and Approximation*, Dover Publications, New York, 1975. 200 pp.

[10] Tobin A. Driscoll, *Algorithm 843: Improvements to the Schwarz–Christoffel Toolbox for MATLAB*, ACM Transactions on Mathematical Software, 31 (2005), pp. 239–251.

[11] Tobin A. Driscoll and Lloyd N. Trefethen, *Schwarz–Christoffel Mapping*, Cambridge University Press, Cambridge, UK, 2002.

[12] C. Engstler, *A port of the FORTRAN code* `radau5` *to MATLAB*, 1999. `http://na.uni-tuebingen.de/na/software.shtml`.

[13] J.M. Floryan, *Conformal-mapping-based coordinate generation method for flows in periodic configurations*, Journal of Computational Physics, 62 (1986), pp. 221–247.

[14] Gene Golub and Victor Pereyra, *Separable nonlinear least squares: the variable projection method and its applications*, Institute of Physics, Inverse Problems, 19 (2003), pp. 1–26.

[15] G. H. Golub and V. Pereyra, *The differentiation of pseudo-inverses and nonlinear least squares problems whose variables separate*, SIAM Journal on Numerical Analysis, 10 (1973), pp. 413–432.

[16] E. Hairer, S. P. Norsett, and G. Wanner, *Solving Ordinary Differential Equations II. Stiff and Differential-Algebraic Problems*, Springer, Berlin, Germany, 1996.

[17] E. Hairer and G. Wanner, *FORTRAN codes that accompany the book [16]*, 2002. `http://www.unige.ch/hairer/software.html`.

[18] Nicholas Hale and Lloyd N. Trefethen, *New quadrature methods from conformal maps*, SIAM Journal of Numerical Analysis, Vol. 46, Issue 2, (2008).

[19] C. T. Kelley, *Solving nonlinear equations with Newton's method*, Fundamentals of Algorithms, SIAM, Philadelphia, PA, 2003.

[20] H. Kober, *Dictionary of Conformal Representations*, Dover, New York, 1952.

[21] Dan Kosloff and Hillel Tal-Ezer, *A modified Chebyshev pseudospectral method with an $O(N^{-1})$ time step restriction*, J. Comput. Phys., 104 (1993), pp. 457–469.

[22] Heinz-Otto Kreiss, N. K. Nichols, and David L. Brown, *Numerical methods for stiff two-point boundary value problems*, SIAM Journal on Numerical Analysis, 23 (1986), pp. 325–368.

[23] Philip Rabinowitz, *Rough and ready error estimates in Gaussian integration of analytic functions*, Commun. ACM, 12 (1969), pp. 268–270.

[24] Gabor Szegő, *Conformal mapping of the interior of an ellipse onto a circle*, The American Mathematical Monthly, 57 (1950), pp. 474–478.

[25] E. Tadmor, *The exponential accuracy of Fourier and Chebyshev differencing methods*, SIAM Journal on Numerical Analysis, 23 (1986), pp. 1–10.

[26] T. W. Tee, *An Adaptive Rational Spectral Method for Differential Equations with Rapidly Varying Solutions*, D.Phil in Numerical Analysis, University of Oxford, 2006. `http://www.comlab.ox.ac.uk/oucl/research/na/thesis/thesistee.pdf`.

[27] T. W. Tee and L. N. Trefethen, *A rational spectral collocation method with adaptively transformed Chebyshev grid points*, SIAM J. Sci. Comput., 28 (2006), pp. 1798–1811.

[28] Lloyd N. Trefethen, *Spectral Methods in MATLAB*, Society for Industrial and Applied Mathematics, Philadelphia, PA, USA, 2000.

[29] ——, *Is Gauss quadrature better than Clenshaw-Curtis?*, SIAM Rev., 50 (2008), pp. 67–87.